Methods of Searching for Higgs and Supersymmetric Particles at the LHC

by

Alan Wah Lun Mak

A dissertation submitted in partial satisfaction of the
requirements for the degree of
Bachelor of Science

in

Physics

in the

COLLEGE OF CREATIVE STUDIES
of the
UNIVERSITY OF CALIFORNIA, SANTA BARBARA

Thesis Advisor:
Professor Jeffrey Richman

Fall 2008

The dissertation of Alan Wah Lun Mak is approved:

Professor Jeffrey Richman Date

Professor Francesc Roig Date

University of California, Santa Barbara

Fall 2008

Methods of Searching for Higgs and Supersymmetric Particles at the LHC

by

Alan Wah Lun Mak

Abstract

Methods of Searching for Higgs and Supersymmetric Particles at the LHC

by

Alan Wah Lun Mak

Bachelor of Science in Physics

University of California, Santa Barbara

Professor Jeffrey Richman, Advisor

With the aid of Monte Carlo event samples, the methods of discovering the Higgs boson and supersymmetric particles at the Large Hadron Collider (LHC) of the European Organization for Nuclear Research (CERN) in Geneva, Switzerland are studied. The study on the Higgs boson is focused on determining the best decay channels for reconstructing the Higgs boson in different mass ranges, which involves examining the dependence of the partial decay widths and the branching fractions on the mass of the Higgs boson. The study on supersymmetric particles is focused on reducing the Standard Model backgrounds to supersymmetry signals, which involves examining the effectiveness of the cuts applied to the event samples.

Acknowledgments

I would like to express many thanks to my thesis advisor Professor Jeffrey Richman for giving me the opportunity to get involved in the exciting research in the UCSB High Energy Physics Group. I am highly indebted to my academic advisor Professor Francesc Roig for his guidance and support throughout my time at UCSB as an undergraduate physics student; and to Professor David Cannell, whose academic advice has always been helpful. Also, I am very grateful to graduate student Mr. Finn Rebessoo in the UCSB High Energy Physics Group, from whom I have learned a lot. Last but not least, I would like to take this opportunity to thank the *Deutsches Elektronen-Synchrotron* (DESY) in Germany and the *Istituto Nazionale di Fisica Nucleare* (INFN) in Italy for enriching my experience in physics research, by giving me the opportunity to participate in their international summer research programmes.

Contents

List of Figures

List of Tables

Chapter 1

Overview

The Large Hadron Collider (LHC) at the European Organization for Nuclear Research (CERN) in Geneva, Switzerland has been officially inaugurated in October 2008. At the LHC, two beams of protons are collided at center-of-mass energy 14 TeV, which is by far the highest energy level ever achieved by any particle collider. In the years to come, the experiments at the LHC will explore this new energy regime, in attempt to search for new particles, to discover new phenomena and to answer some unanswered questions in physics. Two of the most important goals of the experiments at the LHC are to discover the Higgs boson and to discover supersymmetric particles.

The existence of the Higgs boson H is predicted by the Standard Model, and in principle accounts for the masses of elementary particles. However, the Higgs boson has not been observed as of 2008, and the precise value of its mass is still not known. As the Higgs boson is the only missing piece of the Standard Model, the discovery of the Higgs boson would complete the Standard Model.

Meanwhile, the Standard Model is insufficient to account for various phenomena in elementary particle physics. These insufficiencies provide motivations for extending the Standard

Model, and the discovery of the Higgs boson would provide clues for *how* the Standard Model should be extended [1].

An extension of the Standard Model is achieved by the concept of supersymmetry (SUSY). Supersymmetry refers to an invariance of the theory under the interchange of fermions and bosons. It associates an elementary particle with a counterpart, known as the superpartner, whose spin differs by $1/2$ unit. Thus, it predicts the existence of a fermionic superpartner for every boson and a bosonic superpartner for every fermion. This extension of the Standard Model leads to new particles and new interactions.

In the past decades, the physics community has devoted much theoretical effort to the studies of supersymmetry. But as of 2008, there is no experimental evidence for supersymmetry. Various studies have shown that supersymmetric particles will likely be detected at the LHC, and will be revealed by large excesses of events over the expectations of the Standard Model in a number of characteristic signatures [2].

Chapter 2

The Search for the Higgs Boson

2.1 Some Basic Concepts

In elementary particle physics, the decay of a particle is characterized by the *lifetime*. If we have an ensemble of a certain type of particle, then the *individual lifetime* of a particle in the ensemble is the time t elapsed between some reference time and the instant when it decays into another state; and the *mean lifetime* of that type of particles, denoted by the symbol τ, is the arithmetic mean of the individual lifetimes, $\langle t \rangle$.

By the Heisenberg uncertainty principle, $\Delta E \Delta t \approx \hbar$. In the rest frame of a particle, $\Delta E = \Delta(mc^2) = (\Delta m)c^2$ and $\Delta t = \tau$. It follows that [3]

$$\tau \approx \frac{\hbar}{(\Delta m)c^2}. \tag{2.1}$$

Researchers in elementary particle physics often prefer working with natural units, which have $c = \hbar = 1$. We may rewrite equation (2.1) in natural units as

$$\tau \approx \frac{1}{\Delta m}. \tag{2.2}$$

This shows that the lifetime of the particle is inversely proportional to the spread of its mass.

The lifetime of a particle is related to another quantity called the *total decay width*, denoted by the symbol Γ. It is defined as the probability per unit time that a particle decays. Suppose that we have an ensemble of a certain type of particles, and let $N(t)$ be the number of particles in the ensemble as a function of time. Then, the number of particles that decay within a time interval dt is $N\Gamma dt$, and so [3]

$$dN = -N\Gamma dt. \tag{2.3}$$

Integrating both sides of this equation yields [3]

$$N(t) = N(0)e^{-\Gamma t}. \tag{2.4}$$

We can then use this expression to find out the lifetime of this type of particles:

$$\tau = \langle t \rangle = \frac{\int_0^\infty tN(t)\,dt}{\int_0^\infty N(t)\,dt} = \frac{\int_0^\infty te^{-\Gamma t}\,dt}{\int_0^\infty e^{-\Gamma t}\,dt} = \frac{\frac{1}{\Gamma^2}}{\frac{1}{\Gamma}} = \frac{1}{\Gamma} \tag{2.5}$$

It turns out that the total decay width Γ is the reciprocal of the lifetime τ. Therefore, the total decay width of a decay channel actually gives us some information about the *rate* of decay through that channel. From equations (2.2) and (2.5), it follows that

$$\Gamma \approx \Delta m. \tag{2.6}$$

The implication of equation (2.6) is that one can obtain the total decay width of a particle, and hence the lifetime, by finding the spread in the mass. Conversely, the total decay width of a particle can also provide us with information about the mass of the particle.

Furthermore, a particle usually has more than one *decay channels* (also known as *decay modes*). The probablity per unit time that a particle decays through a particular decay channel is

called the *partial decay width* for that channel, and the sum of the partial decay widths Γ_i for all the possible decay channels gives the total decay width Γ. That is, [3]

$$\Gamma = \sum_{i=1}^{n} \Gamma_i. \tag{2.7}$$

Another quantity that is useful in elementary particle physics is the *branching fraction* B_i (often called *branching ratio*) of a decay channel, which is defined as [3]

$$B_i = \frac{\Gamma_i}{\Gamma}. \tag{2.8}$$

The branching fraction is a measure of the fraction that a certain decay channel contributes to all the decay processes [3], and all these fractions sum up to 1. While the partial decay widths for different decay channels are uncorrelated with each other, the branching fractions for different decay channels depend on each other to certain extent. This is because the denominator of equation (2.8), namely Γ, does depend on *all* the possible decay channels of the decaying particle. Moreover, since all branching fractions have to sum up to 1, if the branching fraction of a decay channel increases, those of some other decay channels will be suppressed. The decay channel with the largest branching fraction is the *dominant* decay channel.

2.2 Studying a Method of Discovering the Higgs at the LHC

At the LHC, two beams of protons are set into collision at center-of-mass energy $\sqrt{s} = 14$ TeV. As protons consist of quarks and gluons, myriads of interactions can take place when they are brought together at such a high energy level, thus producing many different particles. The Standard Model predicts that Higgs bosons can be produced through a number of interactions. The dominant [4] process that produces Higgs bosons is gluon-gluon fusion (Fig. 2.1).

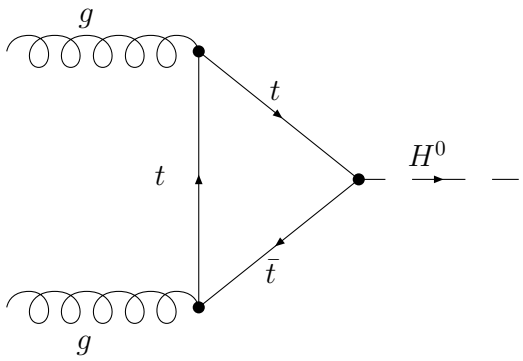

Figure 2.1: The Feynman diagram for the production of a Higgs boson through gluon-gluon fusion

Although the mass of the Higgs boson is still not precisely known, empirical data from previous collider experiments have shown that the lower bound on the mass of the Higgs boson is around 114.4 GeV/c^2 [5]. Due to its high mass, a Higgs boson is expected to decay before it reaches the detector. Therefore, the method to detect the Higgs boson at the LHC is to *reconstruct* it from its decay products by adding up the energy-momentum four-vectors of the decay products found by the detector. To achieve this, it is important to study the decay channels of the Higgs boson and find out which decay channels are the best for this purpose. In the following study, we examine the partial decay widths and the branching fractions of various different decay channels of the Higgs boson. However, since the value of the Higgs mass is not known, we have to consider different possible values of the Higgs mass and find out how these partial decay widths and branching fractions change with the Higgs mass.

2.3 Monte Carlo Event Generation

A computer simulation is conducted, with the aid of a Monte Carlo event generator, to help us understand the dependence of the branching fraction and partial decay width of each decay channel on the mass of the Higgs boson, m_H. The computer simulation is carried out using the Monte Carlo event generator PYTHIA (version 6.319) [6], and the object-oriented data analysis framework ROOT (version 5.10/00) [7] is used for the subsequent analyses.

One feature of PYTHIA is that it allows the user to input the mass of a particle to any desired value. Using the SetPMAS function, the mass of the Higgs boson, m_H, is set to different values ranging from 50 GeV/c^2 to 1000 GeV/c^2 in increments of 10 GeV/c^2, and the subsequent physics is studied. In the simulation for each value of m_H, two beams of protons are first set into collision at center-of-mass energy $\sqrt{s} = 14$ TeV, emulating an experimental condition that matches the condition at the LHC. Gluon-gluon fusion is set to be the production mechanism of the Higgs boson in the computer simulation. Meanwhile, initial state radiation is turned off; but final state radiation, multiple interactions among beam jets and fragmentation are left on. The Higgs bosons produced can then decay into lighter particles through various decay channels. The branching fractions and the partial decay widths of the following 14 decay channels are studied.

$$
\begin{array}{lcl}
H \to d + \bar{d} & , & H \to u + \bar{u} \\
H \to s + \bar{s} & , & H \to c + \bar{c} \\
H \to b + \bar{b} & , & H \to t + \bar{t} \\
H \to e^+ + e^- & , & H \to \mu^+ + \mu^- \\
H \to \tau^+ + \tau^- & , & H \to g + g \\
H \to \gamma + \gamma & , & H \to \gamma + Z \\
H \to Z + Z & , & H \to W^+ + W^-
\end{array}
$$

As the Higgs bosons decay, the branching fraction of each decay channels is obtained by the GetBRAT function in PYTHIA. Meanwhile, the *total* decay width of the Higgs is obtained by

the function GetPMAS(25,2). Using equation (2.8), the *partial* decay width of each decay channel is calculated by multiplying the branching fraction of that channel to the *total* decay width.

2.4 Partial Decay Width Analysis

The partial decay widths of all the Higgs decay channels studied in this computer simulation are plotted, on a logarithmic scale, as a function of the Higgs mass that is input into PYTHIA, ranging from 50 GeV/c^2 to 1000 GeV/c^2 (Fig. 2.2). While the curves for most decay channels increase gradually, those for $H \rightarrow Z + Z$ and $H \rightarrow W^+ + W^-$ increase rather dramatically.

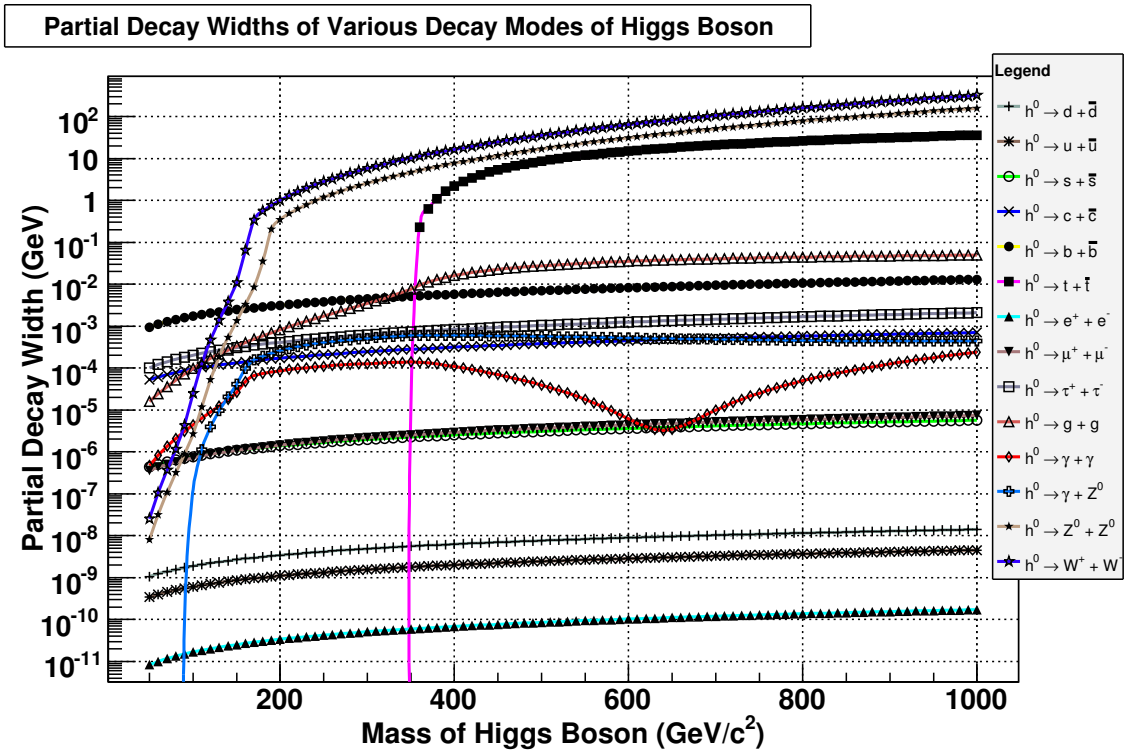

Figure 2.2: A graph showing the partial decay widths of all the Higgs decay channels studied in the computer simulation on a logarithmic scale, and their dependence on the Higgs mass that is input into PYTHIA, ranging from 50 GeV/c^2 to 1000 GeV/c^2

This contrast is more clearly seen in Fig. 2.3 and Fig. 2.4, which are the plots of the same quantities, but on linear scales. In particular, Fig. 2.3 shows that as the mass of the Higgs boson increases, the partial decay width of $H \rightarrow W^+ + W^-$ increases the most rapidly, and is followed by that of $H \rightarrow Z + Z$. Meanwhile, the partial decay widths of the other channels, shown in Fig. 2.4, are smaller than 0.1 GeV, and are very insignificant when compared to those of $H \rightarrow W^+ + W^-$ and $H \rightarrow Z + Z$. Since the partial width of a Higgs decay channel measures the probability per unit time that the Higgs boson decays through that channel, this shows that the decay through channels $H \rightarrow W^+ + W^-$ and $H \rightarrow Z + Z$ are more probable than the others.

It is also worthy to note that the dramatic increase in the partial widths of $H \rightarrow Z + Z$ and

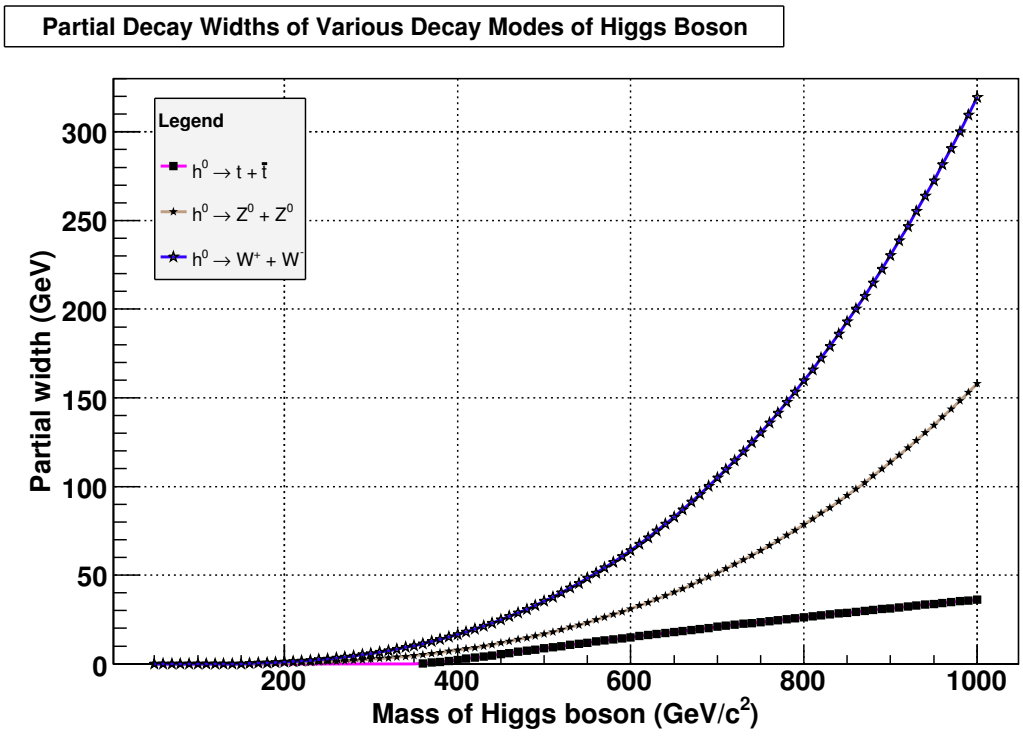

Figure 2.3: A graph showing the partial decay widths, on a linear scale, as a function of the Higgs mass that is input into PYTHIA. The partial decay widths of the other decay channels, which are smaller than 0.1 GeV, are too small to be visible on such a scale.

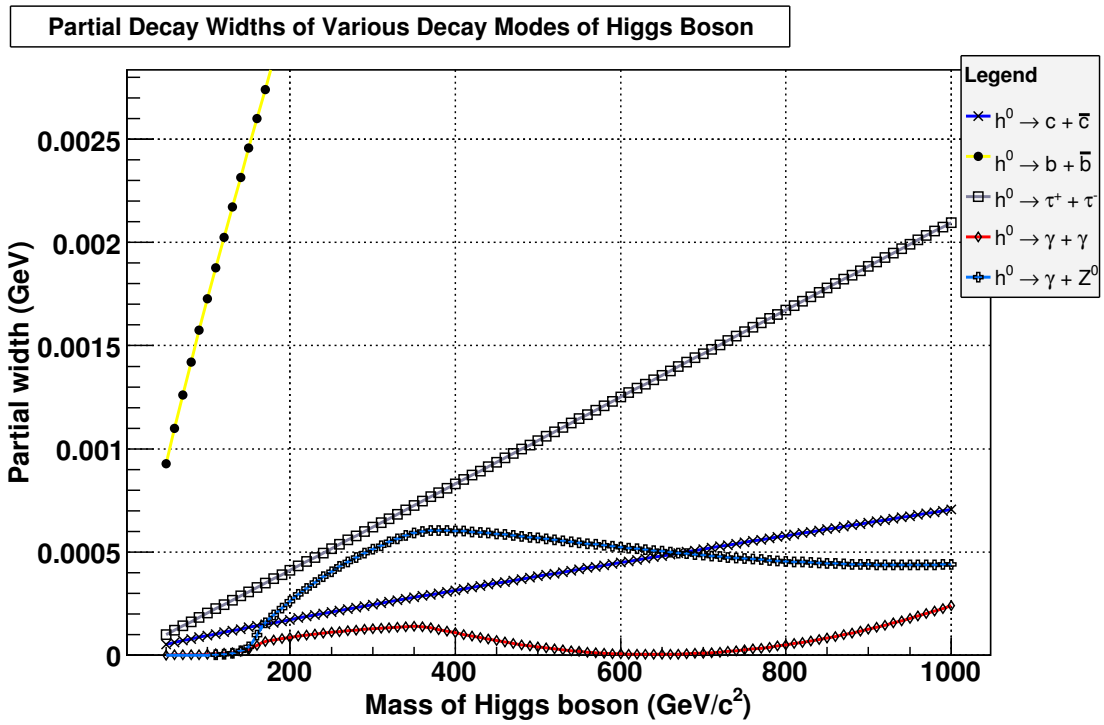

Figure 2.4: Another graph showing the partial decay widths, on a magnified linear scale focusing on the range $0 \leq \Gamma \leq 0.0028$, as a function of the Higgs mass that is input into PYTHIA.

$H \rightarrow W^+ + W^-$ shown in Fig. 2.3 does not occur all the way from m_H = 50 GeV/c^2 to m_H = 1000 GeV/c^2. Instead, they start at certain threshold values. The threshold value for $H \rightarrow W^+ + W^-$ is around m_H = 160 GeV/c^2, which is approximately the total mass of two W bosons; while the threshold value for $H \rightarrow Z + Z$ is around m_H = 180 GeV/c^2, which is approximately the total mass of two Z bosons. In both cases, the thresholds occur when the mass of the Higgs boson reaches the total mass of the products. This effect is due to the fact that when the mass of the Higgs boson is greater than or equal to the total mass of the products, it allows all the products to be on-shell particles, and that is kinematically favourable.

2.5 Branching Fraction Analysis

The branching fractions of all the Higgs decay channels studied in this computer simulation are plotted, on a logarithmic scale, as a function of the Higgs mass that is input into PYTHIA, ranging from 50 GeV/c^2 to 1000 GeV/c^2, as shown in Fig. 2.5. In this figure, it is seen that the branching fractions reach their asymptotic values at high Higgs mass, and all the interesting fluctuations in the branching fractions actually occur at low Higgs mass. Fig. 2.6 shows a zoomed-in version of Fig. 2.5, focusing on the variations of the branching fractions at low Higgs mass, namely 0 GeV/$c^2 \leq m_H \leq$ 600 GeV/c^2.

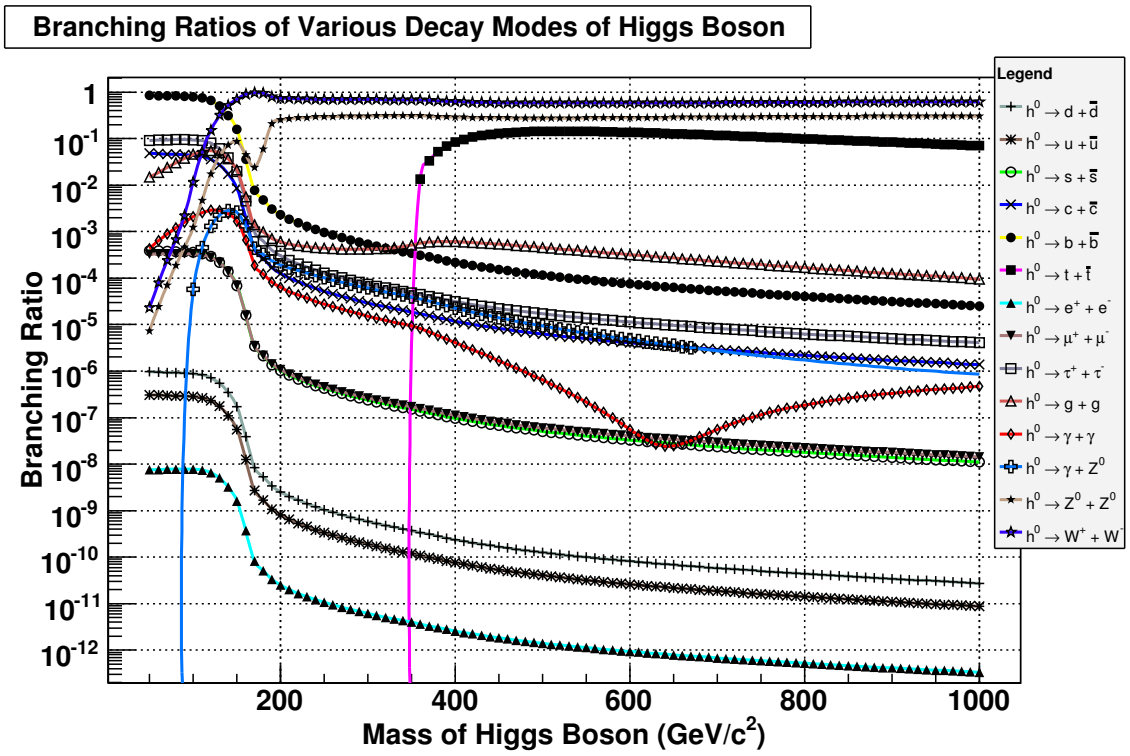

Figure 2.5: A graph showing the branching fractions of all the Higgs decay channels studied in the computer simulation on a logarithmic scale, and their dependence on the Higgs mass that is input into PYTHIA, ranging from 50 GeV/c^2 to 1000 GeV/c^2

From Fig. 2.6, when the Higgs mass is below 80 GeV/c^2, the decay channel $H \rightarrow b + \bar{b}$ has the greatest branching fraction, namely about 0.8, meaning that about 80% of all the decays are in the mode $H \rightarrow b + \bar{b}$. Meanwhile, the decay channel $H \rightarrow \tau^+ + \tau^-$ has the second greatest branching fraction, namely about 0.1, meaning that about 10% of all the decays are in the mode $H \rightarrow \tau^+ + \tau^-$. In this mass range, the other decay channels have branching fractions smaller than 0.1, which are insignificant when compared to those for $H \rightarrow b + \bar{b}$ and $H \rightarrow \tau^+ + \tau^-$. In other words, below 80 GeV/c^2, the *dominant* decay channels are $H \rightarrow b + \bar{b}$ and $H \rightarrow \tau^+ + \tau^-$.

The mass range 100 GeV/$c^2 \leq m_H \leq$ 200 GeV/c^2 is where the branching fractions change the most rapidly. In this mass range, $H \rightarrow b + \bar{b}$ and $H \rightarrow \tau^+ + \tau^-$ cease to be the

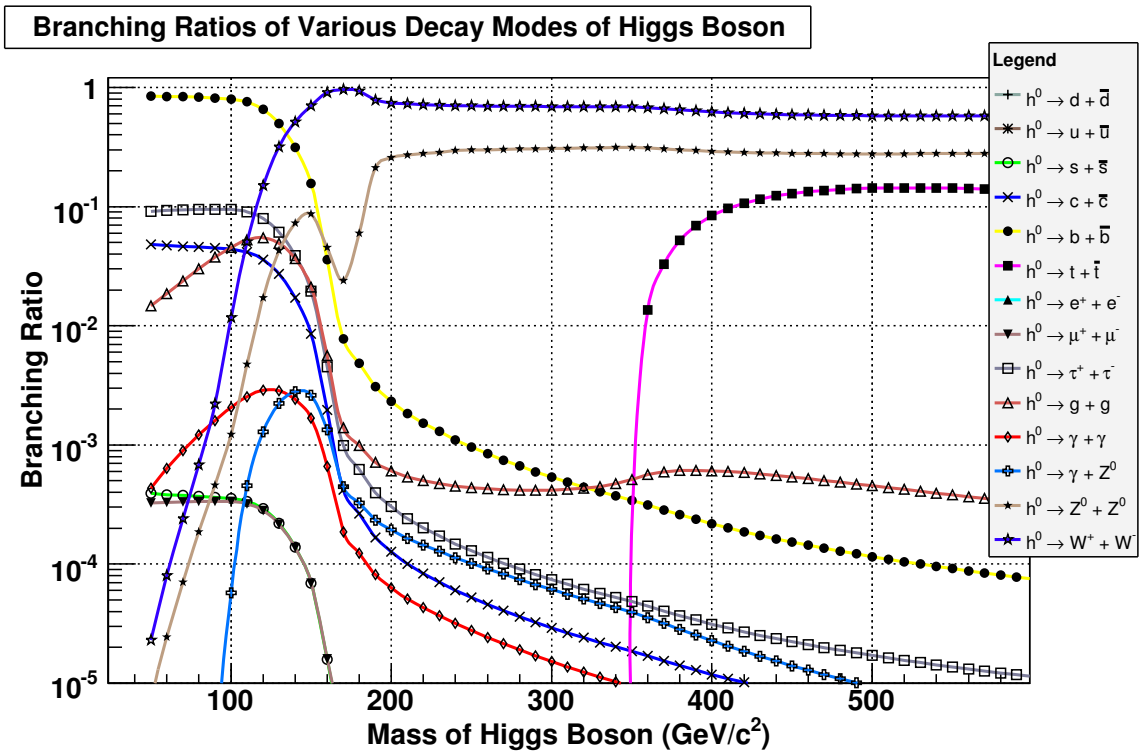

Figure 2.6: A zoomed-in version of Fig. 2.5, focusing on the variations of the branching fractions at low Higgs mass, namely 50 GeV/$c^2 \leq m_H \leq$ 600 GeV/c^2

dominant decay channels, and their branching fractions drop sharply to very small values. The dramatic decrease of these branching fractions is more clearly seen in Fig. 2.7, a plot of the branching fractions on a linear scale.

Meanwhile, the branching fraction for $H \rightarrow W^+ + W^-$ is increasing in this mass range. This is because the *partial width* of $H \rightarrow W^+ + W^-$ starts to increase dramatically at around m_H = 160 GeV/c^2 (Fig. 2.3). On the other hand, the partial widths for the other decay channels do not increase as rapidly. As a result, in equation (2.8), the numerator increases a lot more rapidly than the denominator, thus causing the branching fraction for $H \rightarrow W^+ + W^-$ to rise.

In the same mass range, the curve for $H \rightarrow Z + Z$ has a distinctive "zig-zag" shape. From

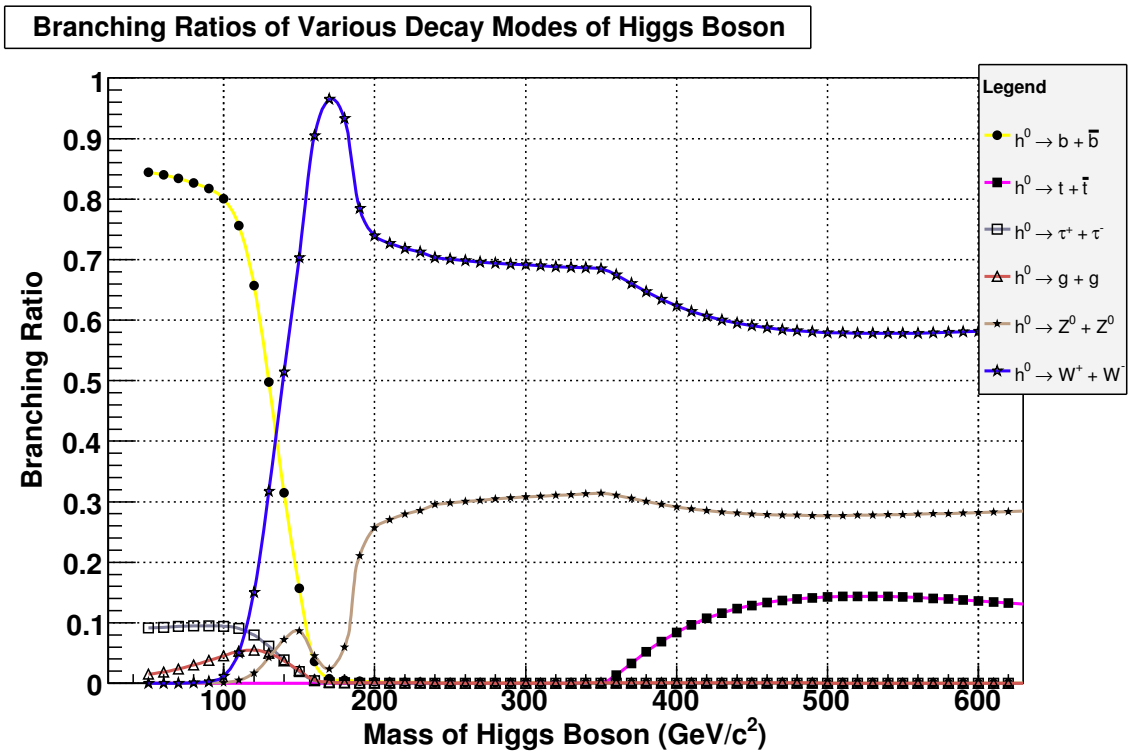

Figure 2.7: A graph showing the branching fractions, on a linear scale, as a function of the Higgs mass that is input into PYTHIA

Fig 2.7, when the branching fraction for $H \rightarrow W^+ + W^-$ reaches its peak at $m_H \approx 170$ GeV/c^2, the branching fractions for all other decay channels drop to nearly zero. However, since the *partial width* for $H \rightarrow Z + Z$ crosses its threshold at $m_H \approx 180$ GeV/c^2 (Fig. 2.3), for the same reason, its branching fraction starts to increase again at $m_H \approx 180$ GeV/c^2. This accounts for the "zig-zag" shape of the curve for $H \rightarrow Z + Z$.

In the mass range, 200 GeV/$c^2 \leq m_H \leq 350$ GeV/c^2, the dominant decay channels are $H \rightarrow W^+ + W^-$ and $H \rightarrow Z + Z$. Their branching fractions are about 0.7 and 0.3, respectively (Fig. 2.7). Meanwhile, all other decay channels have branching fractions smaller than 10^{-2} (Fig. 2.6).

However, at $m_H \approx 350$ GeV/c^2, the branching fraction of $H \rightarrow t + \bar{t}$ starts to increase sharply (Fig. 2.7). Since the branching fractions of all the decay channels have to sum up to 1, this causes the branching fractions of the other decay channels to decrease.

At $m_H \approx 450$ GeV/c^2, the curves for $H \rightarrow W^+ + W^-$, $H \rightarrow Z + Z$ and $H \rightarrow t + \bar{t}$ in Fig. 2.7 begin to level out. As the Higgs mass increases further and the asymptotic values of the branching fractions are reached, $H \rightarrow W^+ + W^-$, $H \rightarrow Z + Z$ and $H \rightarrow t + \bar{t}$ become the dominant decay channels. Their branching fractions are about 0.58, 0.28 and 0.15, respectively (Fig. 2.6). At the same time, the branching fractions of all the other decay channels are smaller than 10^{-3} and become insignificant (Fig. 2.7).

2.6 Conclusion

As the experiments at the LHC attempt to discover the Higgs boson by reconstructing it from its decay products, it is important to select appropriate decay channels for this purpose. One

Table 2.1: The dominant decay channels of the Higgs boson in different mass ranges

Higgs mass (GeV/c^2)	Dominant decay channels
50 - 100	$H \rightarrow b + \bar{b}$, $H \rightarrow \tau^+ + \tau^-$, $H \rightarrow g + g$
100 - 150	$H \rightarrow b + \bar{b}$, $H \rightarrow W^+ + W^-$, $H \rightarrow Z + Z$
150 - 350	$H \rightarrow W^+ + W^-$, $H \rightarrow Z + Z$
350 - 1000	$H \rightarrow W^+ + W^-$, $H \rightarrow Z + Z$, $H \rightarrow t + \bar{t}$

of the important selection criteria is that the decay channels have a large branching fractions, which can provide sufficient data and make the discovery possible. Table 2.1 summarizes the dominant decay channels of the Higgs boson in different mass ranges. In terms of large branching fraction, $H \rightarrow b + \bar{b}$ would be the preferable decay channel at low Higgs mass, while $H \rightarrow W^+ + W^-$ and $H \rightarrow Z + Z$ would be the preferable decay channels at high Higgs mass.

However, in addition to large branching fraction, the cleanliness of the final state is also an important criterion for selecting a decay channel for Higgs reconstruction. Due to large irreducible backgrounds, $H \rightarrow b + \bar{b}$ is not efficient for the purpose of searching for the Higgs boson. In this regard, it turns out that $H \rightarrow \gamma + \gamma$ is important for low-mass Higgs search [8], even though its branching fraction is always smaller than 10^{-2} (Fig. 2.6).

Our studies also show that if the mass of the Higgs boson turns out to be much higher than the lower bound 114.4 GeV/c^2 [5], the decay channel $H \rightarrow Z + Z$ has relatively large branching fraction. Furthermore, the process $H \rightarrow ZZ \rightarrow \mu^+\mu^-\mu^+\mu^-$ has very clean final state, in the sense that the backgrounds are not significant. Thus, it is often regarded as the "golden mode" [9] for the discovery of Higgs bosons at the LHC.

Chapter 3

The Search for Supersymmetric Particles

3.1 History of Supersymmetry

The beginning of supersymmetry dated back to the early 1970s, when it was discovered independently by three groups of scientists [10].

The first publication [11] on space-time global supersymmetry was made by Yuri Golfand and Evgeny Likhtman in Moscow, Russia in 1971, at about the same time when world-sheet two-dimensional symmetry in string theories was observed [12]. The two scientists found the extension of the Poincaré algebra and constructed a theory of supersymmetric quantum electrodynamics (QED) with the mass term of the photon/photino fields and two chiral matter superfields [13].

Shortly after, Dmitry Volkov and Vladimir Akulov published [14] on their independent formulation of the four-dimensional super-Poincaré algebra in Kharkov, Ukraine in 1972. Based

on a non-linear realization of the algebra, they wrote down a geometrical Lagrangian for the self-interaction of the Goldstone fermion of supersymmetry, in attempt to account for the masslessness of the neutrino in exact analogy to the masslessness of the pion in the limit of spontaneously broken chiral symmetry in quantum chromodynamics (QCD) [15].

At that time, the publications of these scientists were only available in Soviet Journals in Russian, and were not noticed by the wider physics community [10]. Unaware of the previous work, Julius Wess (in Karlsruhe, Germany) and Bruno Zumino (at CERN in Geneva, Switzerland) collaborated on the theory of supersymmetry in a different approach. Their formalism of supersymmetry in four dimensions was inspired by the world-sheet symmetry of the Neveu-Ramond-Schwarz fermionic strings [15], and was published [16] in 1974. Their work had boosted the interest of the physics community in Lagrangian field theory and in elementary particle physics [15].

It is worth noting that while most conceptual developments in science were the consequence of the attempts to account for some known facts about nature or some unexpected empirical observations, the discovery of supersymmetry in the 1970s was "a purely intellectual achievement, driven by the logic of theoretical development rather than by the pressure of existing data" [12].

The innovations in 1981 by Savas Dimopoulos and Howard Georgi [17] marked another important milestone in the theoretical development of supersymmetry. In response to the famous "hierarchy problem" [18], the two scientists proposed the idea of soft supersymmetry breaking and constructed the Minimal Supersymmetric Standard Model (MSSM), which is by far the only significant quantitative success in any extension of the Standard Model [19].

3.2 The Minimal Supersymmetric Standard Model

The Minimal Supersymmetric Standard Model (MSSM) is the simplest extension of the Standard Model, in the sense that it has minimal particle content. This supersymmetric extension of the Standard Model provides a natural way of incoporating elementary scalar particles (such as the Higgs boson) into the framework of quantum field theory [20].

3.2.1 Particle Content

As an *extension* of the Standard Model, the MSSM contains all the particles in the Standard Model, namely quarks, leptons, gauge bosons and Higgs bosons. Meanwhile, this supersymmetric extension associates each of these Standard Model particles with a superpartner, whose spin differs by $1/2$ unit, thus doubling the total number of particles. These superpartners, known as *sparticles*, fall into the five categories:

- **squarks** ($\tilde{q}$) — superpartners of quarks (q),
- **sleptons** ($\tilde{l}$) — superpartners of leptons (l),
- **neutralinos** ($\tilde{B}^0$, $\tilde{W}^0$, $\tilde{H}_u^0$, $\tilde{H}_d^0$) — superpartners of neutral bosons (B^0, W^0, H_u^0, H_d^0),
- **charginos** ($\tilde{W}^{\pm}$, $\tilde{H}_u^+$, $\tilde{H}_d^-$) — superpartners of charged bosons ($W^{\pm}$, H_u^+, H_d^-),
- **gluinos** ($\tilde{g}$) — superpartners of gluons (g).

While quarks and leptons in the Standard Model are collectively known as *fermions*, their superpartners, squarks and sleptons, are collectively known as *sfermions*. It should be noted that a fermion (f) has spin $1/2$, and hence two chirality states (a left-handed state and right-handed state). Upon the supersymmetric extension, these two chirality states correspond to two distinct sfermions, $\tilde{f}_L$ and $\tilde{f}_R$, which are scalars.

Besides, bosons can be classified into *gauge bosons* (B^0, W^0, $W^{\pm}$), which are force carriers, and *Higgs bosons* (H_u^0, H_d^0, H_u^+, H_d^-), which give mass to other particles via the Higgs Mechanism [21]. Their superpartners in the MSSM are the *gauginos* ($\tilde{B}^0$, $\tilde{W}^0$, $\tilde{W}^{\pm}$) and the *higgsinos* ($\tilde{H}_u^0$, $\tilde{H}_d^0$, $\tilde{H}_u^+$, $\tilde{H}_d^-$), respectively. With electroweak symmetry breaking, the B^0 and W^0 gauge eigenstates mix to form mass eigenstates Z^0 and γ; the corresponding gaugino mixtures of the *bino* ($\tilde{B}^0$) and the *wino* ($\tilde{W}^0$) are the *zino* ($\tilde{Z}^0$) and the *photino* ($\tilde{\gamma}$).

The particle content of the MSSM is summarized in Table 3.1.

Table 3.1: A summary of the particle content of the Minimal Supersymmetric Standard Model

Standard Model particles			Corresponding superpartners			
Category	Particles	Spin	Category	Particles		Spin
				Gauge eigenstates	Mass eigenstates	
quarks	$u\ d$	$\frac{1}{2}$	*squarks*	$\tilde{u}_L\ \tilde{u}_R\ \tilde{d}_L\ \tilde{d}_R$	$*$	0
	$c\ s$			$\tilde{c}_L\ \tilde{c}_R\ \tilde{s}_L\ \tilde{s}_R$	$*$	
	$t\ b$			$\tilde{t}_L\ \tilde{t}_R\ \tilde{b}_L\ \tilde{b}_R$	$\tilde{t}_1\ \tilde{t}_2\ \tilde{b}_1\ \tilde{b}_2$	
leptons	$e\ \nu_e$	$\frac{1}{2}$	*sleptons*	$\tilde{e}_L\ \tilde{e}_R\ \tilde{\nu}_e$	$*$	0
	$\mu\ \nu_\mu$			$\tilde{\mu}_L\ \tilde{\mu}_R\ \tilde{\nu}_\mu$	$*$	
	$\tau\ \nu_\tau$			$\tilde{\tau}_L\ \tilde{\tau}_R\ \tilde{\nu}_\tau$	$\tilde{\tau}_1\ \tilde{\tau}_2\ \tilde{\nu}_\tau$	
neutral bosons	$B^0\ W^0$	1	*neutralinos*	$\tilde{B}^0\ \tilde{W}^0$	$\tilde{N}_1\ \tilde{N}_2\ \tilde{N}_3\ \tilde{N}_4$	$\frac{1}{2}$
	$H_u^0\ H_d^0$	0		$\tilde{H}_u^0\ \tilde{H}_d^0$		
charged bosons	$W^{\pm}$	1	*charginos*	$\tilde{W}^{\pm}$	$\tilde{C}_1^{\pm}\ \tilde{C}_2^{\pm}$	$\frac{1}{2}$
	$H_u^+\ H_d^-$	0		$\tilde{H}_u^+\ \tilde{H}_d^-$		
gluons	g	1	*gluinos*	$\tilde{g}$	$*$	$\frac{1}{2}$

$*$ indicates that the mass eigenstates are identical to the gauge eigenstates.

3.2.2 Mass Spectrum

For squarks and sletpons, the mass eigenstates are formed by the mixings among the up-type squarks ($\tilde{u}_L$, $\tilde{c}_L$, $\tilde{t}_L$, $\tilde{u}_R$, $\tilde{c}_R$, $\tilde{t}_R$), among the down-type squarks ($\tilde{d}_L$, $\tilde{s}_L$, $\tilde{b}_L$, $\tilde{d}_R$, $\tilde{s}_R$, $\tilde{b}_R$), among the charged sleptons ($\tilde{e}_L$, $\tilde{\mu}_L$, $\tilde{\tau}_L$, $\tilde{e}_R$, $\tilde{\mu}_R$, $\tilde{\tau}_R$) and among the sneutrinos ($\tilde{\nu}_e$, $\tilde{\nu}_\mu$, $\tilde{\nu}_\tau$). For the first- and second-generation squarks and sleptons, the mixings are not substantial. As a result, the gauge eigenstates are, to a good approximation [21], also the mass eigenstates. However, for the third-generation squarks and sleptons, the effect of Yukawa couplings [21] is not negligible. Also, the off-diagonal elements between left and right states in the mass matrices, which are proportional to the masses of the corresponding fermions [21], are not negligible. Therefore, new mass eigenstates are formed by the mixing in pairs, ($\tilde{t}_L$, $\tilde{t}_R$), ($\tilde{b}_L$, $\tilde{b}_R$) and ($\tilde{\tau}_L$, $\tilde{\tau}_R$).

For neutralinos and charginos, the mass eigenstates are formed by the mixing between higgsinos and electroweak gauginos. The mass eigenstates $\tilde{N}_i$ ($i = 1, 2, 3, 4$) of neutralinos are formed by the combinations of the neutral higgsinos ($\tilde{H}_u^0$ and $\tilde{H}_d^0$) and the neutral gauginos ($\tilde{B}^0$ and $\tilde{W}^0$), while the eigenstates $\tilde{C}_i$ ($i = 1, 2$) of charginos are formed by the combinations of the charged higgsinos ($\tilde{H}_u^+$ and $\tilde{H}_d^-$) and the charged gauginos ($\tilde{W}^+$ and $\tilde{W}^-$). The mass eigenstates $\tilde{N}_i$ and $\tilde{C}_i$ are labeled such that the mass increases with the value of i.

For gluinos, the mass eigenstates are the same as the colour octet, because they cannot mix with any other particle in the MSSM.

3.2.3 The Lightest Supersymmetric Particle

The lightest supersymmetric particle (LSP) refers to a stable particle in the MSSM into which all the other supersymmetric particles eventually decay. The lightest neutralino $\tilde{N}_1$ is usually

assumed to be the LSP.

The existence of the LSP is an implication of the conservation of R-parity P_R in the MSSM. R-parity is also known as matter parity. It is a multiplicative quantum number. All Standard Model particles, including the Higgs bosons, have even parity ($P_R = +1$); while all supersymmetric particles, such as squarks, sleptons, gauginos and higgsinos, have odd parity ($P_R = -1$). The conservation of R-parity in the MSSM requires that there is no mixing between odd and even R-parity particles, and that every interaction vertex in the model contains an even number of odd R-parity particles. As a result, each sparticle (except the LSP) must eventually decay into a state that contains an odd number of LSPs (usually just one) [21].

The lightest neutralino $\tilde{N}_1$, which is assumed to be the LSP, is a good candidate [10, 22] for cold dark matter, which comprises non-baryonic particles with non-relativistic motion. The reason is three-fold. First, $\tilde{N}_1$ is electrically neutral, and does not participate in electromagnetic interactions. Thus, it does not scatter light, and is highly invisible. Second, $\tilde{N}_1$ is colourless, so it does not participate in strong interaction either. Therefore, it is only subject to weak nuclear force and gravitational force, which have much weaker strength than strong nuclear force and electromagnetic force. This accounts for its stability. Third, $\tilde{N}_1$ is expected to be very massive compared to Standard Model particles – otherwise it would have already been detected in previous particle collider experiments. The high mass of $\tilde{N}_1$ precludes its motion from being relativistic.

3.3 Production of Supersymmetric Particles at the LHC

At the LHC, two proton beams are set into collision at center-of-mass energy 14 TeV. If the sparticles predicted by the MSSM actually exist, they will likely [2] be detected at the LHC.

Since protons consist of quarks and gluons, the following strong interactions are expected to be the dominant production mechanisms for sparticles at the LHC: [20, 21]

- **gluon-gluon fusion** ($gg \rightarrow \tilde{g}\tilde{g}$, $gg \rightarrow \tilde{q}\bar{\tilde{q}}$),
- **gluon-quark fusion** ($gq \rightarrow \tilde{g}\tilde{q}$),
- **quark-antiquark annihilation** ($q\bar{q} \rightarrow \tilde{g}\tilde{g}$, $q\bar{q} \rightarrow \tilde{q}\bar{\tilde{q}}$),
- **quark-quark scattering** ($qq \rightarrow \tilde{q}\tilde{q}$).

The corresponding Feynman diagrams for these sparticle production mechanisms are shown in Fig. 3.1. As these interactions have QCD strength, they can produce squarks and gluinos with large cross sections. The squarks and gluinos produced can then decay into other sparticles, leading to many possible decay chains.

In particular, a gluino ($\tilde{g}$) can decay into a squark ($\tilde{q}$) through strong interaction. A squark can carry out electroweak decay and yield a neutralino ($\tilde{N}_i$) or a chargino ($\tilde{C}_i$). Neutralinos and charginos can further decay and produce a wide variety of other sparticles. For instance, they can decay into charged sleptons ($\tilde{l}$), sneutrino ($\tilde{\nu}$) and gauge bosons ($W^{\pm}$, Z) through eletroweak interactions; they can also decay into Higgs bosons (h^0, H^0, A^0, $H^{\pm}$) through the Higgs Mechanism. The decay chain ends when the lightest supersymmetric particle $\tilde{N}_1$ is reached. The possible decay vertices of each type of sparticles is summarized in Table 3.2.

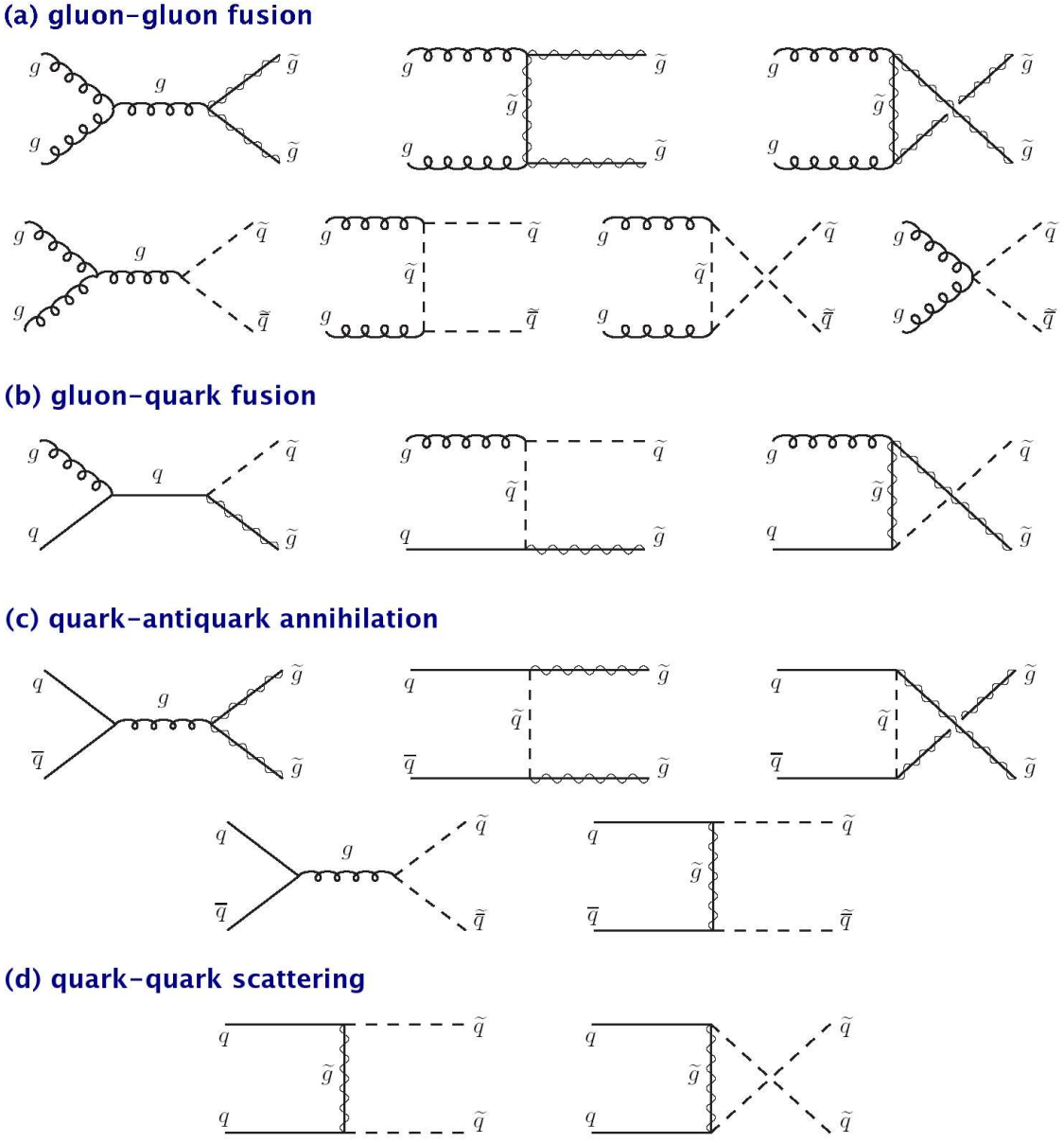

Figure 3.1: The Feynman diagrams for the production of sparticles at the LHC through (a) gluon-gluon fusion, (b) gluon-quark fusion, (c) quark-antiquark annihilation and (d) quark-quark scattering. (This figure is based on fig. 9.1-9.3 in ref. [21].)

Table 3.2: A summary of the possible decay vertices in the Minimal Supersymmetric Standard Model

Sparticle	Decay vertex	Type of interaction	Sparticle	Decay vertex	Type of interaction
Gluino	$\tilde{g} \rightarrow q\tilde{q}$	Strong	Slepton	$\tilde{l} \rightarrow l\tilde{N}_i$	Electroweak
Squark	$\tilde{q} \rightarrow q\tilde{g}$	Strong		$\tilde{l} \rightarrow \nu\tilde{C}_i$	Electroweak
	$\tilde{q} \rightarrow q\tilde{N}_i$	Electroweak		$\tilde{\nu} \rightarrow \nu\tilde{N}_i$	Electroweak
	$\tilde{q} \rightarrow q'\tilde{C}_i$	Electroweak		$\tilde{\nu} \rightarrow l\tilde{C}_i$	Electroweak
Neutralino	$\tilde{N}_i \rightarrow Z\tilde{N}_j$	Electroweak	Chargino	$\tilde{C}_i \rightarrow Z\tilde{C}_j$	Electroweak
	$\tilde{N}_i \rightarrow W\tilde{C}_j$	Electroweak		$\tilde{N}_i \rightarrow W\tilde{N}_j$	Electroweak
	$\tilde{N}_i \rightarrow l\tilde{l}$	Electroweak		$\tilde{N}_i \rightarrow l\tilde{\nu}$	Electroweak
	$\tilde{N}_i \rightarrow \nu\tilde{\nu}$	Electroweak		$\tilde{N}_i \rightarrow \nu\tilde{l}$	Electroweak
	$\tilde{N}_i \rightarrow q\tilde{q}$	Electroweak		$\tilde{N}_i \rightarrow q\tilde{q}'$	Electroweak
	$\tilde{N}_i \rightarrow h^0\tilde{N}_j$	Higgs Mechanism		$\tilde{N}_i \rightarrow h^0\tilde{C}_j$	Higgs Mechanism
	$\tilde{N}_i \rightarrow A^0\tilde{N}_j$	Higgs Mechanism		$\tilde{N}_i \rightarrow A^0\tilde{C}_j$	Higgs Mechanism
	$\tilde{N}_i \rightarrow H^0\tilde{N}_j$	Higgs Mechanism		$\tilde{N}_i \rightarrow H^0\tilde{C}_j$	Higgs Mechanism
	$\tilde{N}_i \rightarrow H^{\pm}\tilde{C}_j^{\mp}$	Higgs Mechanism		$\tilde{N}_i \rightarrow H^{\pm}\tilde{N}_j$	Higgs Mechanism

3.4 Signatures for Supersymmetric Particle Detection at the LHC

As already discussed in the previous section, the Minimal Supersymmetric Standard Model (MSSM) predicts that every sparticle will eventually decay into the lightest supersymmetric particle (LSP), which is assumed to be the lightest neutralino $\tilde{N}_1$. Since this particle has feeble interaction with matter, it escapes the detector, thus leaving a distinctive signature of 'missing energy' (denoted by $\not{E}_T$). Therefore, the observable signals for supersymmetry are, in general, n lepton(s) + m jet(s) + $\not{E}_T$, where either n or m might be zero [21]. Here a "jet" refers to a collimated bunch of hadrons and other particles produced by the hadronization of a quark or gluon in a collider experiment.

It should be noted that many of these signals have significant Standard Model backgrounds [21]. For instance, the W-bosons and the Z-boson have decay vertices $W \rightarrow l\nu$ and $Z \rightarrow \nu\nu$. The neutrinos (ν) produced in these processes will also escape the detector and give rise to 'missing energy' signatures. Therefore, it is important to target appropriate observable signals for which the backgrounds can be reduced, and devise effective methods to reduce the backgrounds.

The 'classical' signature for supersymmetry is an event with large missing energy $\not{E}_T$ and no energetic isolated leptons, which comes from the direct decay of gluinos into the LSP $\tilde{N}_1$ [20]. Other examples of the favourable discovery modes for supersymmetry at the LHC are same-charge dilepton signature [23], which has two leptons with the same charge in the final state, together with jets and $\not{E}_T$; opposite-charge dilepton signature [24], which has two leptons with opposite charges in the final state, together with jets and $\not{E}_T$; and trilepton signature [25], which has three leptons in the final state, together with jets and $\not{E}_T$.

3.5 Studying a Method of Discovering Supersymmetric Particles at the LHC

As the observable signals for sparticles at the LHC are accompanied by significant Standard Model backgrounds, it is important for experimenters to adopt effective methods to reduce these backgrounds. One of the most widely used technique for background reduction is to apply suitable cuts to the data. To examine the effectiveness of this technique, a cut-based analysis is performed on the skimmed Monte Carlo event samples generated by our group.

The Monte Carlo event samples of our group are generated in the CMSSW_1_6_12 framework [26] with the aid of layer 0, layer 1 and the cross cleaner of the Physics Analysis Toolkits

(PAT) [27]. One sample considered in this study is the "LM1" sample, which contains signals of supersymmetry. "LM1" is one of the "low-mass" test points defined by the Compact Muon Solenoid (CMS) Collaboration of CERN, with the values of the five free parameters in the mSUGRA model of supersymmetry specified as follows: [28]

- $m_0 = 60$,
- $m_{1/2} = 250$,
- $\tan\beta = 10$,
- $sign(\mu) = +$,
- $A_0 = 0$.

If this "low-mass" point actually exists in nature, it is expected to be discovered at the LHC with a relatively small integrated luminosity [29]. Another sample considered in this study is the "muon chowder" sample, which contains the Standard Model backgrounds $t\bar{t}$ + jets, W + jets and Z + jets. The total number of events in the LM1 sample is 120,624, while the total number of events in the muon chowder sample is 4,477,207. Within the muon chowder sample, there are 312,252 $t\bar{t}$ + jets events, 3,106,884 W + jets events and 1,058,071 Z + jets events.

3.6 Cut-based Analysis

3.6.1 Description of the Cuts

Our group has written a C++ macro that applies cuts on the LM1 sample and muon chowder sample. The cuts applied in this study are modeled after those in the study performed by the CMS group in Aachen, Germany. These cuts are detailed in ref. [29] and are summarized as follows.

- **C**ut 1: Muon high level triggers
    - (a) HLT1MuonIso
    - (b) HL2MuonIso
    - (c) HL2MuonNonIso
- **C**ut 2: Muon acceptance and identification criteria
    - (a) $p_T(\mu) \geq 20$ GeV/c
    - (b) Tracker isolation criteria $\sum_{\Delta R<0.3} p_T(\text{track}) < 6$ GeV/c
    - (c) Number of tracker hits ≥ 12
    - (d) $\chi^2/N_{dof} < 3$
    - (e) $|\eta(\mu)| < 2.1$ rad
- **C**ut 3: Jet acceptance criteria
    - (a) $|\eta(\text{jet})| \geq 2.5$ rad
    - (b) Percentage of jet energy reconstructed in the hadron calorimeter $\geq 10\%$
    - (c) Top 3 leading jets have $p_T \geq 80$ GeV/c
- **C**ut 4: Preselection missing energy $\not\!\!E_T \geq 100$ GeV
- **C**ut 5: Criteria on angular distributions
    - (a) $|\Delta\phi(\mu, \not\!\!E_T)| > 0.8$ rad
    - (b) $|\Delta\phi(\text{leading jet}, \not\!\!E_T)| > 0.6$ rad
    - (c) $|\Delta\phi(2^{nd}\text{ leading jet}, \not\!\!E_T)| > 0.6$ rad
    - (d) $|\Delta\phi(3^{rd}\text{ leading jet}, \not\!\!E_T)| > 0.6$ rad
- **C**ut 6: $p_T(\text{leading jet}) \geq 200$ GeV/c
- **C**ut 7: $p_T(2^{nd}\text{ leading jet}) \geq 150$ GeV/c

- **C**ut 8: Final missing energy $\not{E}_T \geq 250$ GeV

3.6.2 Results and Analysis

As the C++ macro applies cuts to the LM1 sample and muon chowder samples, it also records the number of SUSY (LM1) events, the number of $t\bar{t}$ + jets events, the number of W + jets events and the number of Z + jets events passing each cut. The number of each kind of events passing each cut is then normalized to 1 fb^{-1}, and is presented in Table 3.3.

In the table, the efficiency of each cut is also shown in parentheses. Here the efficiency of a cut is defined as the ratio of the number of events passing the cut to the number of events passing the previous cut. It is worth noting that the Z + jets background has zero event at 1 fb^{-1} after all the eight cuts, meaning that it is totally eliminated by the cuts. Meanwhile, the W + jets background has 2.76 events at 1 fb^{-1} after all the eight cuts, which shows that it is almost totally eliminated by the cuts.

To demonstrate that a cut has been successfully applied to the samples, the distribution of the quantity of interest is plotted right before the cut and right after the cut for comparison. Fig. 3.2 shows the number of muons per event immediately before cuts 1 and 2 are applied (left) and the number of muons satisfying the criteria of cuts 1 and 2 immediately after cuts 1 and 2 are applied (right). The two plots show an overall decrease in the number of muons per event for both the signal (LM1) and the backgrounds ($t\bar{t}$ + jets, W + jets and Z + jets) after cuts 1 and 2. Fig. 3.3 shows the transverse momenta of all muons before cuts 1 and 2 (left) and the transverse momenta of all the remaining muons after cuts 1 and 2 (right). In particular, the plot on the right clearly shows that there are no more muons with transverse momentum lower than 20 GeV/c after cuts 1 and 2.

Fig. 3.4 shows the number of jets (with $p_T > 30$ GeV/c) per event immediately before

Table 3.3: Number of events at integrated luminosity 1 fb^{-1} after each cut (with the efficiency of each cut in parentheses).

Cut	SUSY (LM1) signal	$t\bar{t}$ + jets background	W + jets background	Z + jets background
No cuts	6.11×10^4	1.36×10^5	7.97×10^6	1.30×10^6
1	8.88×10^3 (14.5%)	1.24×10^5 (91.2%)	7.90×10^6 (99.1%)	1.28×10^6 (98.5%)
2	5.43×10^3 (61.1%)	9.80×10^4 (79.0%)	6.30×10^6 (79.7%)	1.05×10^6 (82.0%)
3	2.15×10^3 (39.6%)	1.05×10^4 (10.7%)	3.34×10^3 (0.0530%)	7.32×10^2 (0.0697%)
4	1.96×10^3 (91.2%)	3.56×10^3 (33.9%)	8.95×10^2 (26.8%)	5.40×10^1 (7.38%)
5	8.37×10^2 (42.7%)	9.22×10^2 (25.9%)	2.42×10^2 (27.0%)	6.01×10^0 (11.1%)
6	6.84×10^2 (81.7%)	3.44×10^2 (37.3%)	1.29×10^2 (53.3%)	3.81×10^0 (63.4%)
7	5.38×10^2 (78.7%)	2.14×10^2 (62.2%)	9.74×10^1 (75.5%)	3.28×10^0 (86.1%)
8	3.45×10^2 (64.1%)	1.29×10^1 (6.03%)	2.76×10^0 (2.83%)	0.00×10^0 (0.00%)

cut 3 (left) and the number of jets (with $p_T > 30$ GeV/c) satisfying the criteria of cut 3 immediately after cut 3 (right). These two plots show an overall decrease in the number of jets per event for both the signal (LM1) and the backgrounds ($t\bar{t}$ + jets, W + jets and Z + jets) after cut 3. Fig. 3.5 shows the transverse momenta of the three leading jets in each event before cut 3 (left) and the transverse momenta of the three leading jets in each event after cut 3 (right). In particular, the plot on the right clearly shows that after cut 3 none of the top three leading jets have transverse momentum lower than 80 GeV/c.

Fig. 3.6 is a comparison of the "missing transvere energy" (MET) $\not{E}_T$ immediately before (left) and immediately after (right) cut 4. The two plots are otherwise identical except that all the

events with $\not\!\!E_T$ below 100 GeV are seen in the plot on the left, but are not seen in the plot on the right. This verifies that cut 4 has been successfully applied to the samples.

Figs. 3.7, 3.8, 3.9 and 3.10 show the effects of cut 5 on the angular correlations $|\Delta\phi(\mu, \not\!\!E_T)|$, $|\Delta\phi(\text{leading jet}, \not\!\!E_T)|$, $|\Delta\phi(2^{nd}\text{ leading jet}, \not\!\!E_T)|$ and $|\Delta\phi(3^{rd}\text{ leading jet}, \not\!\!E_T)|$, respectively. It should be noted that for each of these four figures, the plot on the right hand side shows the situation after the cut criteria for *all the four* angular correlations – (a), (b), (c) and (d) – have been applied. These four figures clearly demonstrate that there are no more events with $|\Delta\phi(\mu, \not\!\!E_T)|$ less that 0.8 rad, with $|\Delta\phi(\text{leading jet}, \not\!\!E_T)|$ less than 0.6, with $|\Delta\phi(2^{nd}\text{ leading jet}, \not\!\!E_T)|$ less than 0.6 or with $|\Delta\phi(3^{rd}\text{ leading jet}, \not\!\!E_T)|$ less than 0.6 after cut 5.

Fig. 3.11 shows the distribution of the transverse momentum of the leading jet in each event immediately before (left) and immediately after (right) cut 6 is applied. Fig. 3.12 shows the distribution of the transverse momentum of the 2^{nd} leading jet in each event immediately before (left) and immediately after (right) cut 6 is applied. Fig. 3.13 shows the distribution of the MET $\not\!\!E_T$ immediately before (left) and immediately after (right) cut 8 is applied. These three figures demonstrate that cuts 6, 7 and 8 are successfully applied to the samples, and further show that the three cuts have effectively eliminated the original peaks of the $t\bar{t}$ + jets background.

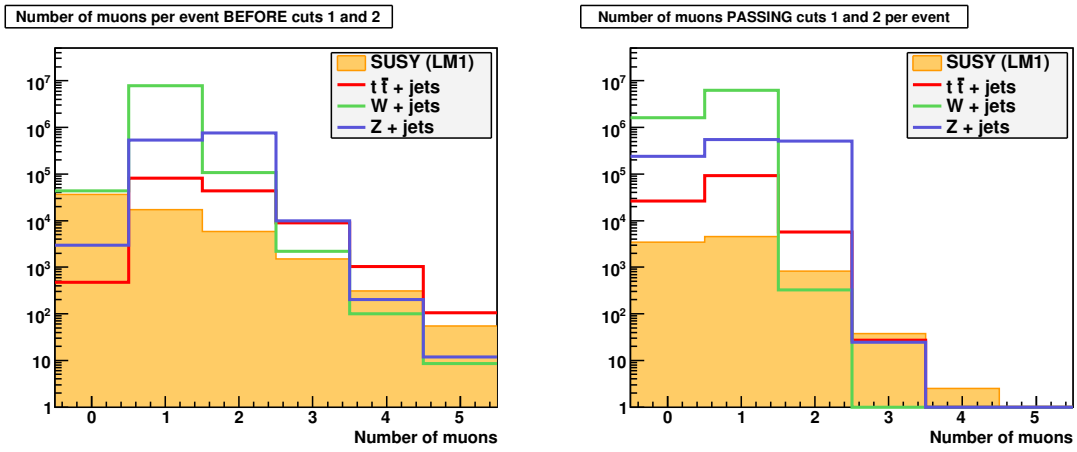

Figure 3.2: The number of muons per event immediately before (left) and immediately after (right) cuts 1 and 2

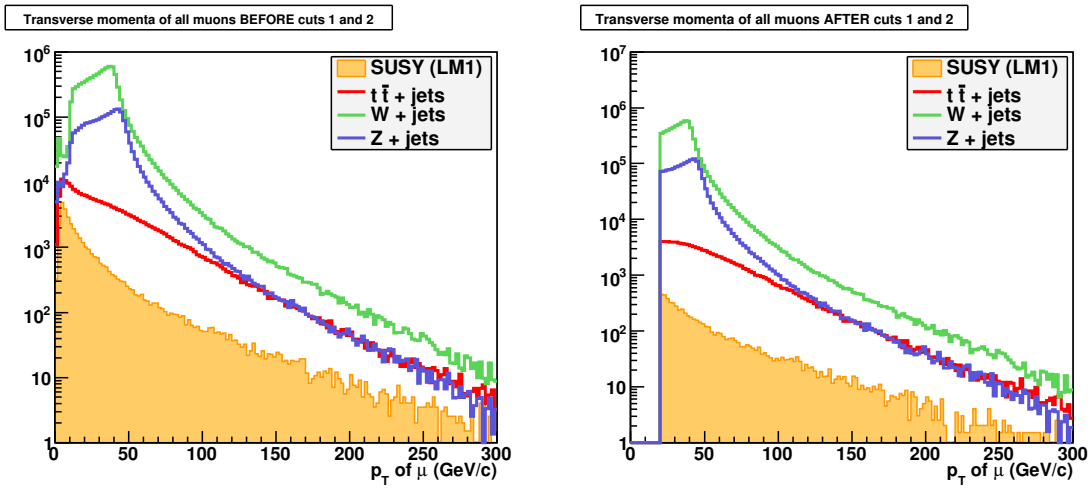

Figure 3.3: The transverse momenta of all muons immediately before (left) and immediately after (right) cuts 1 and 2

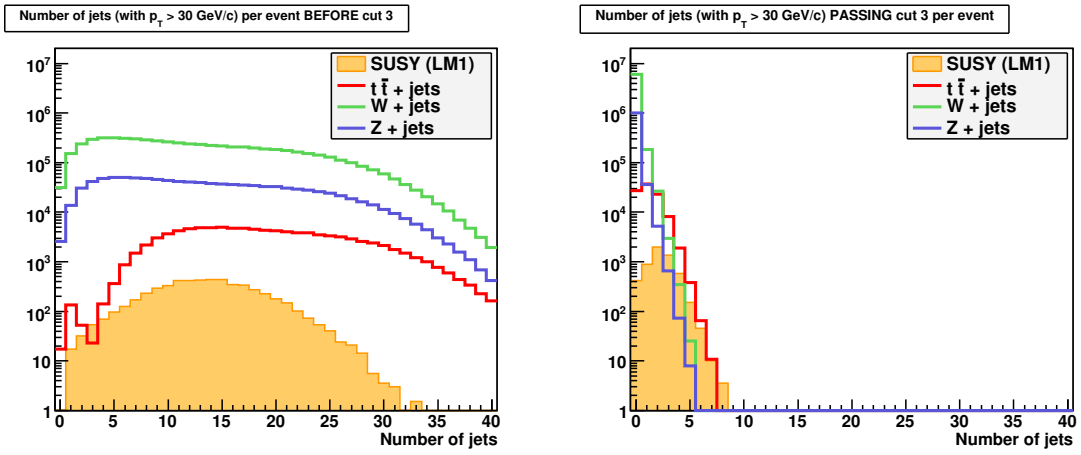

Figure 3.4: The number of jets per event immediately before (left) and immediately after (right) cut 3

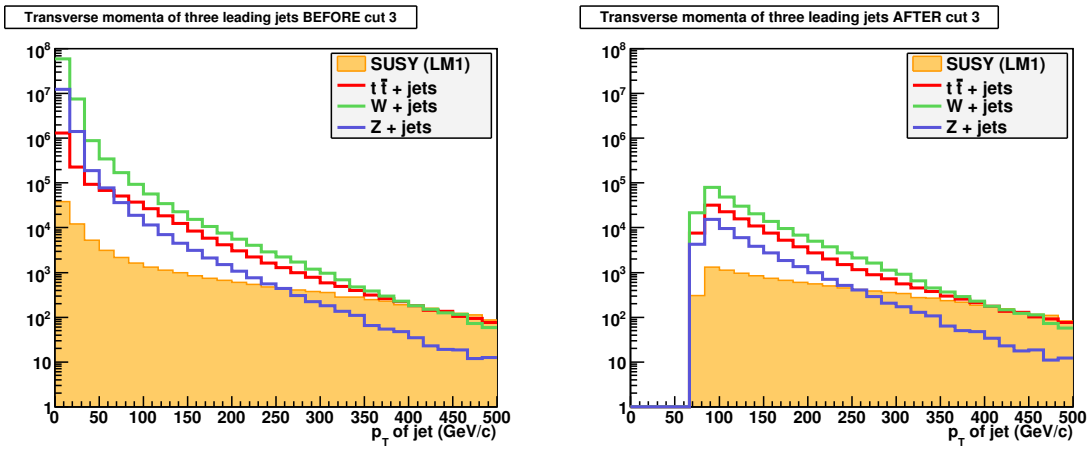

Figure 3.5: The transverse momenta of the three leading jets in each event immediately before (left) and immediately after (right) cut 3

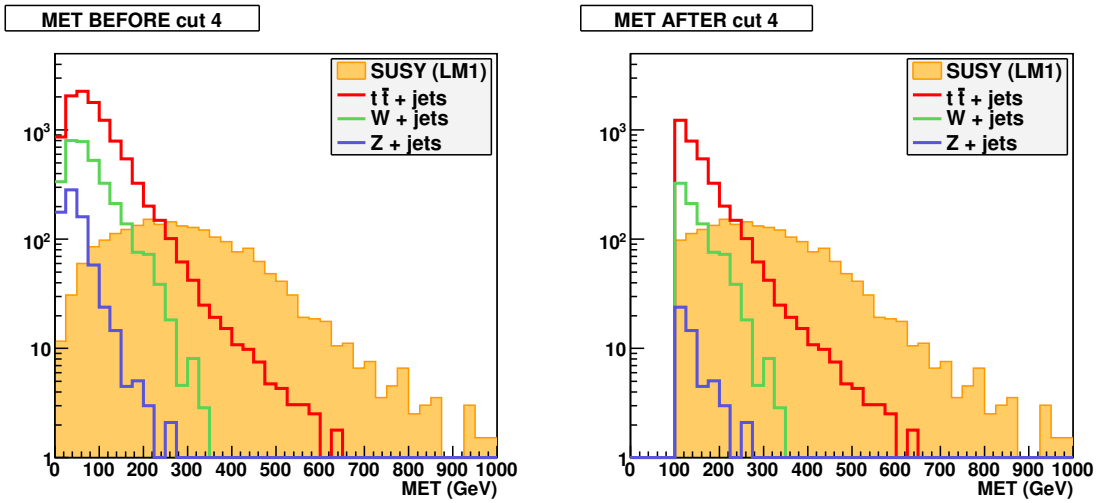

Figure 3.6: The MET immediately before (left) and immediately after (right) cut 4

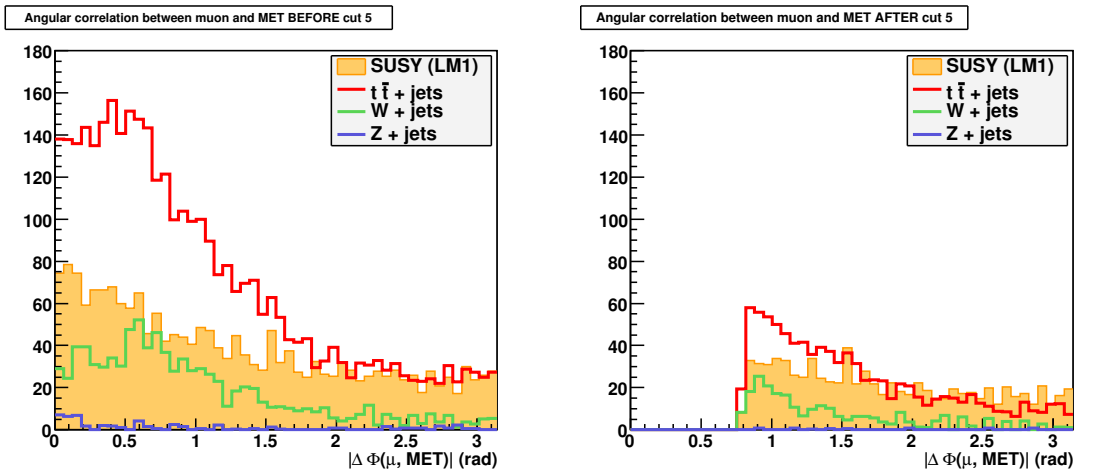

Figure 3.7: The angular correlation between each muon and the MET before (left) and immediately after (right) cut 5

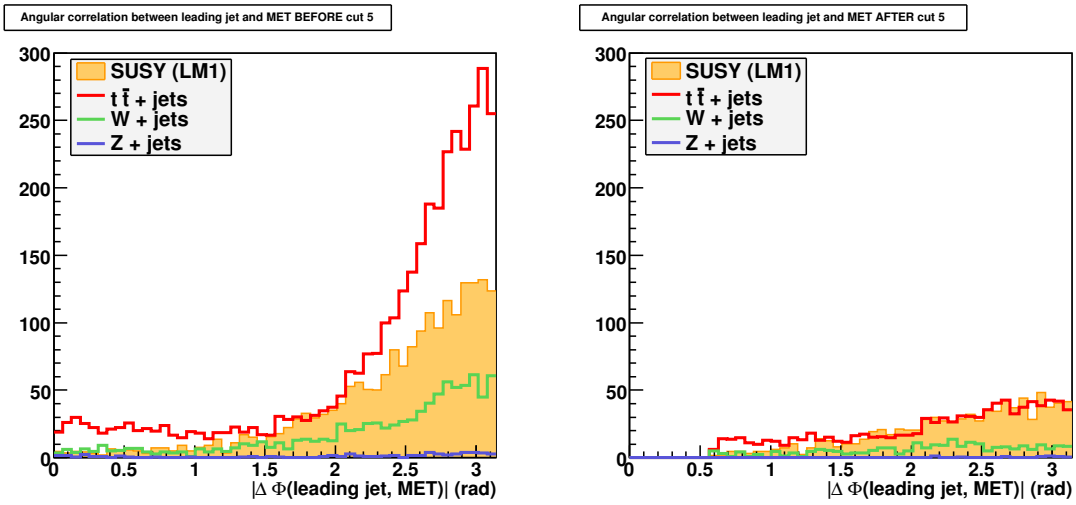

Figure 3.8: The angular correlation between the leading jet and the MET before (left) and immediately after (right) cut 5

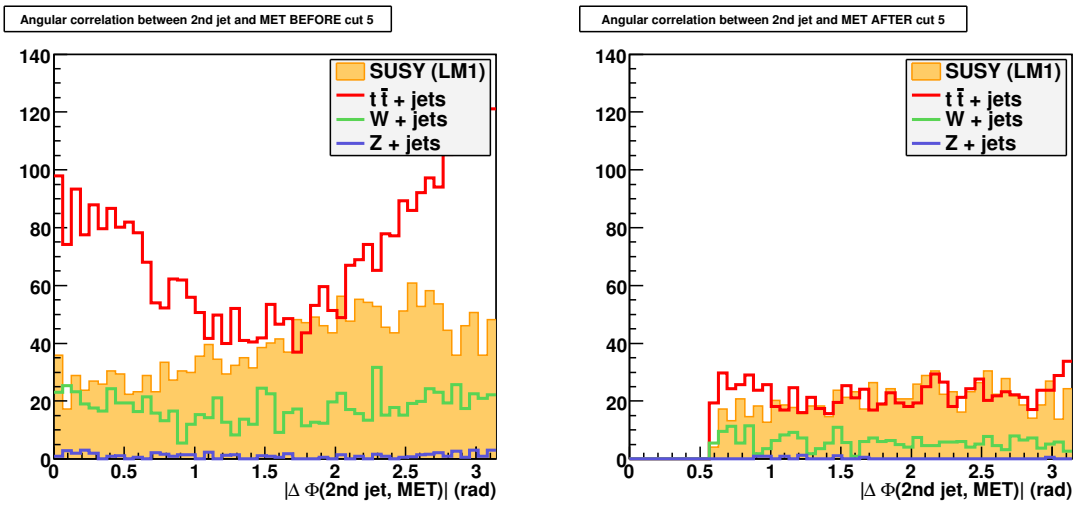

Figure 3.9: The angular correlation between the 2^{nd} leading jet and the MET before (left) and immediately after (right) cut 5

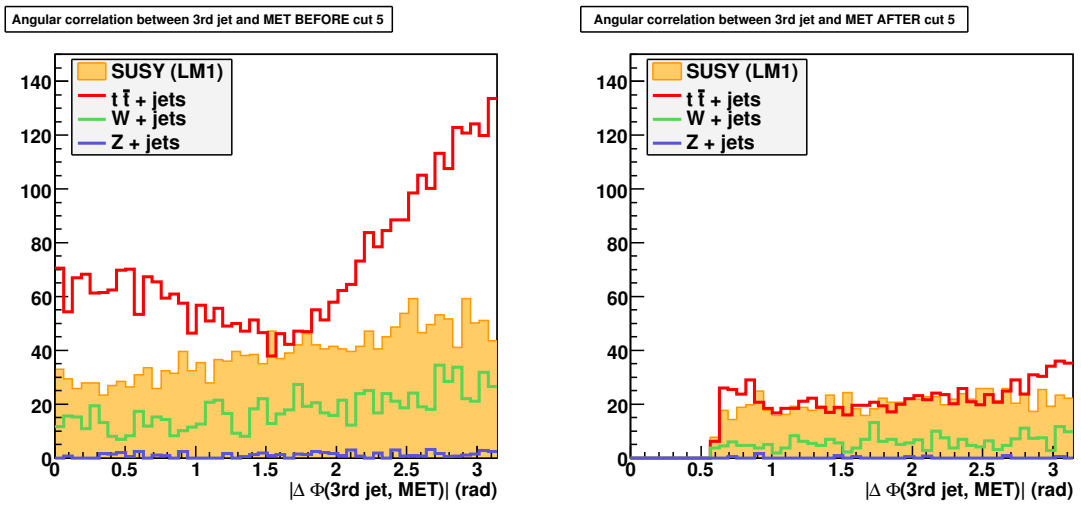

Figure 3.10: The angular correlation between the 3^{rd} leading jet and the MET before (left) and immediately after (right) cut 5

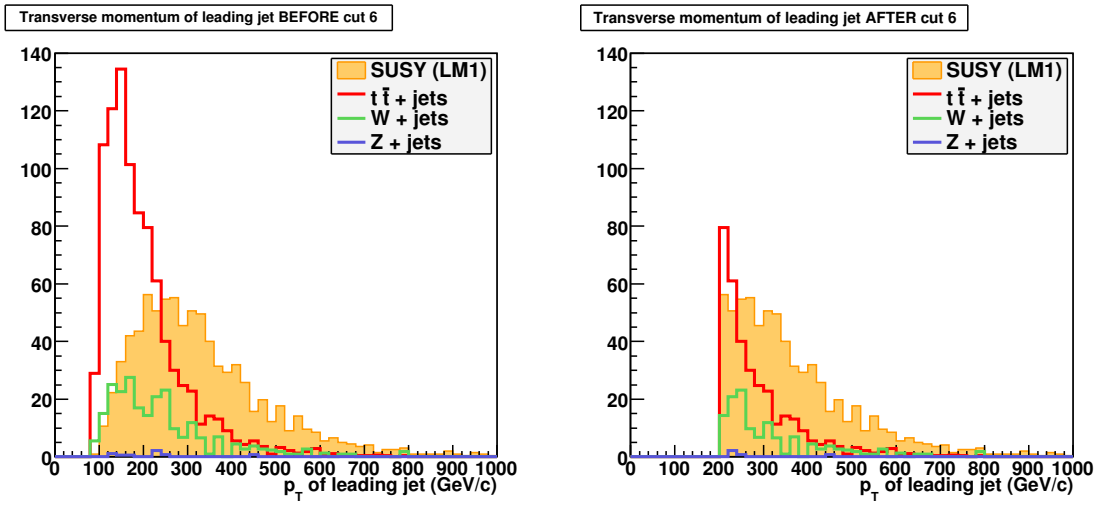

Figure 3.11: The transverse momentum of the leading jet before (left) and immediately after (right) cut 6

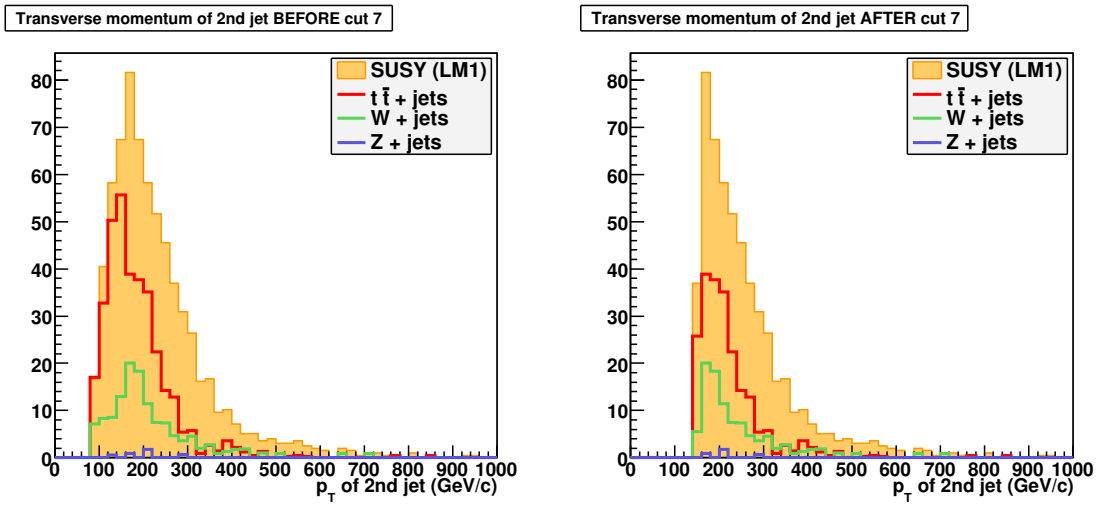

Figure 3.12: The transverse momentum of the 2^{nd} leading jet before (left) and immediately after (right) cut 7

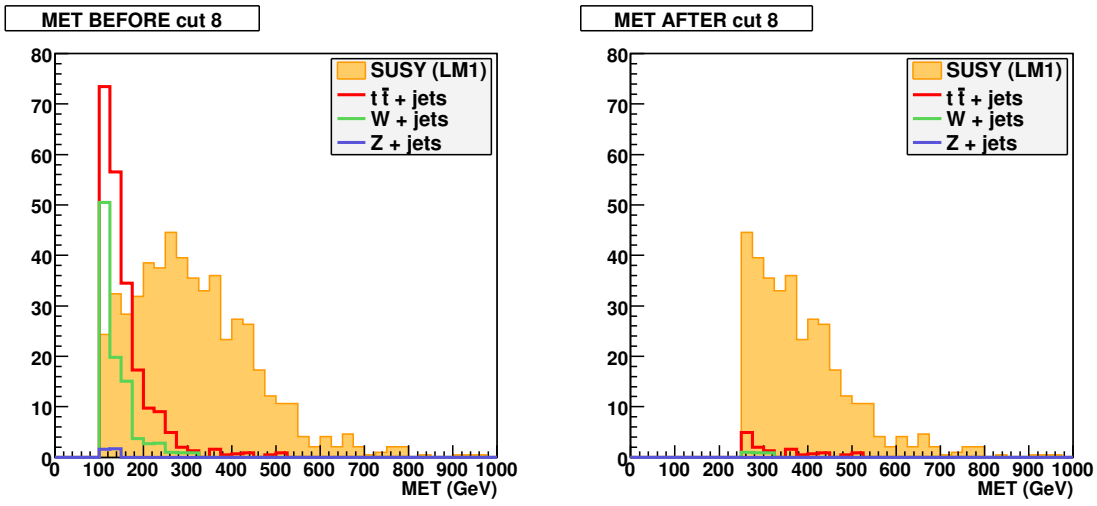

Figure 3.13: The MET immediately before (left) and immediately after (right) cut 8

3.7 Conclusion

In this study, the eight cuts described in the previous section are successfully applied to the LM1 sample and the muon chowder sample generated by our group. The cuts are intended to minimize the Standard Model backgrounds $t\bar{t}$ + jets, W + jets and Z + jets, so as to make the discovery of supersymmetric particles possible. The effectiveness of these cuts are reflected by Figs. 3.14, 3.15 and 3.16, which compare the distributions of three selected quantities before and after *all* the eight cuts. The three selected quantities are, respectively, the MET, the number of jets with $p_T > 30$ GeV/c per event and the transverse momenta p_T of all jets. All three figures clearly show that the $t\bar{t}$ + jets, W + jets and Z + jets backgrounds are significantly reduced by the eight cuts. In particular, at integrated luminosity of 1 fb^{-1}, the Z + jets background is *totally* eliminated.

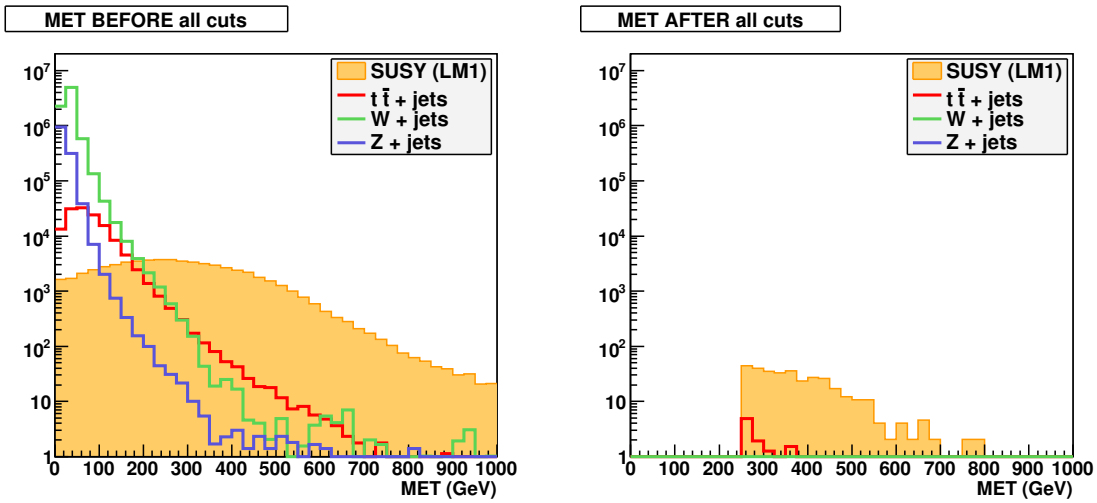

Figure 3.14: The MET before (left) and after (right) all the eight cuts

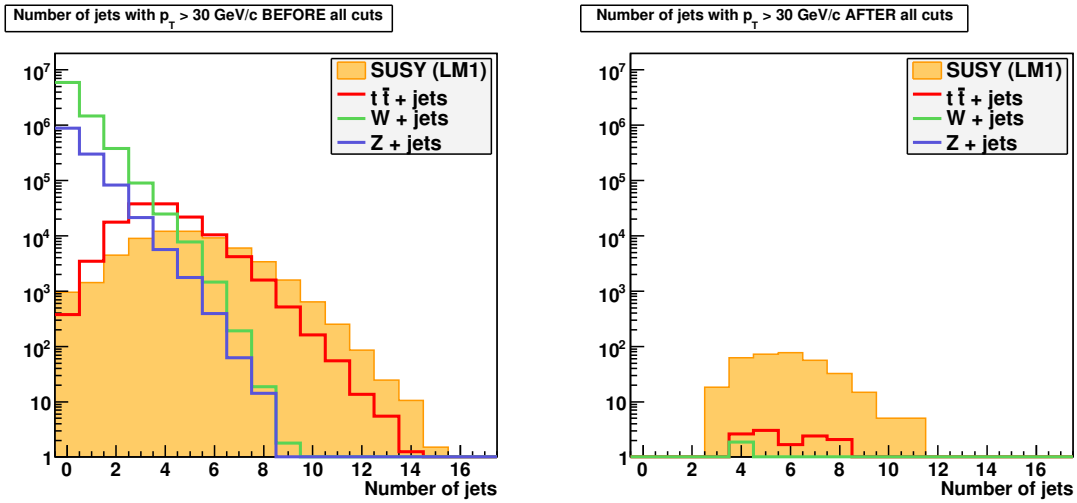

Figure 3.15: The number of jets (with $p_T > 30$ GeV/c) per event before (left) and after (right) all the eight cuts

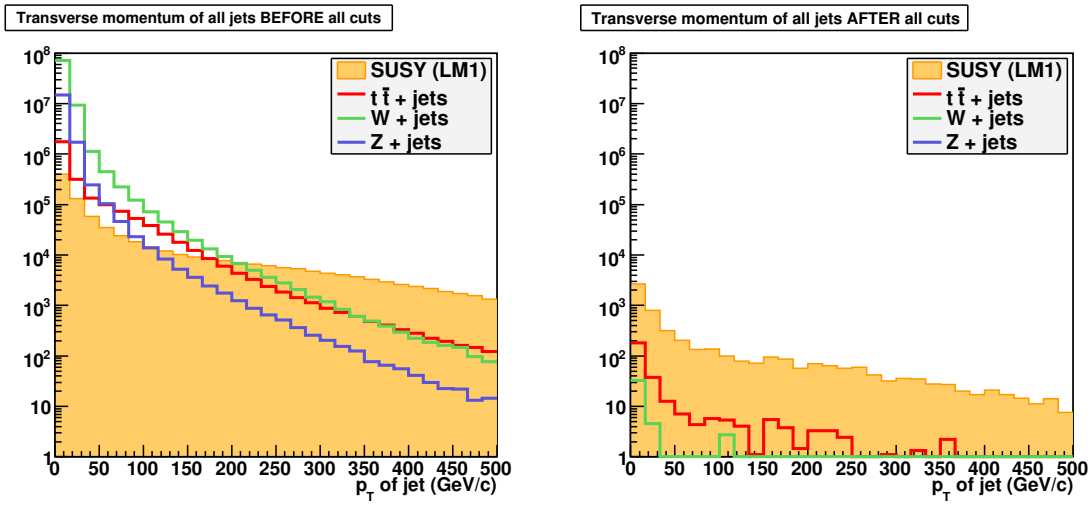

Figure 3.16: The transverse momenta p_T of all jets before (left) and after (right) all the eight cuts

Bibliography

[1] G. L. Kane and E. Witten, "Supersymmetry: Squarks, Photinos, and the Unveiling of the Ultimate Laws of Nature," (Da Capo Press, 2001).

[2] S. Abdullin *et al.*, "Discovery potential for supersymmetry in CMS," *J. Phys. G: Nucl. Part. Phys.* **28** (2002), 469.

[3] I. C. Brock, "Lifetime, Cross-Section and Luminosity," Lecture notes for a course on Elementary Particle Physics at the Universität Bonn, Germany in summer 2007, Chapter 3, *http://pi.physik.uni-bonn.de/~brock/teaching/tp1_ss07/chapter03.pdf*

[4] D. Green, "Vector Boson Fusion Higgs Production at the LHC - Mass Variables," arXiv:hep-ex/0501027v1

[5] The ALEPH, DELPHI, L3, OPAL Collaborations and the LEP Working Group for Higgs Boson Searches, "Search for the Standard Model Higgs boson at LEP," *Phys. Lett.* **B** 565 (2003), 61.

[6] The official homepage of PYTHIA: *http://www.thep.lu.se/~torbjorn/Pythia.html*

[7] The official homepage of ROOT: *http://root.cern.ch/*

[8] Q. Ingram, "The Lead Tungstate Electromagnetic Calorimeter of CMS," Proceedings of the Particles and Nuclei International Conference in Santa Fe, New Mexico in 2005, PACS: R29.40.Mc; 29.40.Vj

[9] A. Drozdetskiya, "CMS detector sensitivity to the Standard Model Higgs boson in $H \rightarrow ZZ^{(*)} \rightarrow 4$ leptons decay channel," *Nucl. Phys.* **B** 177-178 (2008), 283-284.

[10] M. Gaillard and B. Zumino, "Supersymmetry and Superstring Phenomenology," Lawrence Berkeley National Laboratory, Paper LBNL-371E (2008).

[11] Yu. A. Golfand and E. P. Likhtman, "Extension of the Algebra of Poincaré Group Generators and Violation of P Invariance," *JETP Lett.* **13** (1971), 323.

[12] G. L. Kane and M. Shifman, "The Supersymmetric World: The Beginnings of the Theory," (World Scientific, Singapore, 2000).

[13] M. Shifman (ed.), "The Many Faces of Superworld", Yuri Golfand Memorial Volume (World Scientific, Singapore, 2000).

[14] D. V. Volkov and V. P. Akulov, "Is the Neutrino a Goldstone Particle?" *JETP Lett.* **16** (1972), 438.

[15] S. Ferrara (ed.), "Supersymmetry," Volume 1, (North Holland and World Scientific, 1987).

[16] J. Wess and B. Zumino, "Supergauge Transformations in Four Dimensions," *Nucl. Phys.* B **70** (1974), 39.

[17] S. Dimopoulos and H. Georgi, "Softly Broken Supersymmetry and SU(5)," *Nucl. Phys.* B **193** (1981), 150.

[18] E. Gildener, "Gauge-symmetry hierarchies," *Phys. Rev.* D **14** (1976), 1667.

[19] S. Dimopoulos, "Soft Supersymmetry Breaking and the Supersymmetric Standard Model," arXiv:hep-th/0105034v1.

[20] A. Bartl, W. Majerotto and B. Mößlacher, "Production and Decay of Supersymmetric Particles at Future Colliders," Proceedings of a series of seminars held at the Max-Planck-Institut für Physik in Munich, Germany from May to November in 1991.

[21] S. P. Martin, "A Supersymmetry Primer," arXiv:hep-ph/9709356v4.

[22] F. D. Steffen, "Supersymmetric Dark Matter Candidates - The Lightest Neutralino, the Gravitino, and the Axino," Max-Planck-Institut für Physik, Paper MPP-2007-165.

[23] H. Dreiner, Manoranjan Guchait and D. P. Roy, "Like sign dilepton signature for gluino production at the CERN LHC with or without R conservation,", *Phys. Rev.* D **49** (1994), 3270.

[24] M. Chiorboli, M. Galanti and A. Tricomi, "SUSY Searches with Opposite Sign Dileptons at CMS," *Acta Physica Polonica* B **38** (2007), Issue 2, 559.

[25] S. I. Bityukov and N. V. Krasnikov, "Gaugino pair production at LHC for the case of nonuniversal gaugino masses," *Nuovo Cim.* A **112** (1999) 913.

[26] Details of the CMSSW framework can be found at *https://twiki.cern.ch/twiki/bin/view/CMS/SWGuide*

[27] Details of the Physics Analysis Toolkit (PAT) can be found at *https://twiki.cern.ch/twiki/bin/view/CMS/SWGuidePAT*

[28] CMS Collaboration, "CMS Physics Technical Design Report," Volume II, CERN-LHCC-2006-021 (2006), Chapter 13.

[29] P. Biallass *et al.*, "Search Strategies for mSUGRA in the Muons + Jets + MET Final State," CMS Analysis Note AN-2008/034.